



## Journal of Advanced Research in Fluid Mechanics and Thermal Sciences

Journal homepage:  
[https://semarakilmu.com.my/journals/index.php/fluid\\_mechanics\\_thermal\\_sciences/index](https://semarakilmu.com.my/journals/index.php/fluid_mechanics_thermal_sciences/index)  
ISSN: 2289-7879



# An Experimental Study of the Transfer of Heat in Nanofluid of a Tiny-Channel using Several Innovative Arrangement Designs

Ameer Abed Jaddoa<sup>1,\*</sup>, Mahmoud Mustafa Mahdi<sup>1</sup>, Hussain Saad Abd<sup>1</sup>, Jafaar Mohamme Daif<sup>1</sup>

<sup>1</sup> Electromechanical Engineering Department, University of Technology, Baghdad 00964, Iraq

### ARTICLE INFO

#### Article history:

Received 15 October 2023

Received in revised form 9 March 2024

Accepted 20 March 2024

Available online 15 April 2024

#### Keywords:

Mini-channels; new configuration models; TiO<sub>2</sub> nanofluid; heat transfer

### ABSTRACT

This work presents an experimental investigation of the heat transfer (HT) and pressure drop characteristics associated with three different configuration models of minichannel heat sinks. This study utilizes a coolant consisting of TiO<sub>2</sub> nanoparticles dispersed in water at a weight concentration of 10%. The performance of this nanofluid coolant is then evaluated and compared to that of distilled water under several heating powers ranging from 100 to 300 W. The findings suggest that the thermal performance of TiO<sub>2</sub> nanofluid is significantly influenced by heating power (HP), and its HT efficiency can be enhanced more efficiently at lower levels of HP. However, it has been observed that when the HP decreases, the pressure drop increases. This effect is more pronounced in TiO<sub>2</sub> nanofluid than in pure water, which can be attributed to the difference in viscosity with temperature. The Nusselt number remains constant regardless of the increase or reduction in HP. Consequently, when pure water is utilized, the experimental Nusselt number aligns with the Peng and Peterson empirical correlation for all HPs, with an accuracy of 15%. The TiO<sub>2</sub> nanofluid was used to test the lowest wall temperature, 40 °C. This measurement was obtained at a Reynolds number of 1100, equivalent to a heat power (HP) of 100 W. Furthermore, it is noted that when the fluid passes through the mini channel, there is an increase in the axial temperature from the input to the outlet of the heat sink (HS). The maximum enhancement observed for a power input of 100 W is 19.59% when utilizing configuration A. This is attributed to the combination of a weak buoyancy force and an increase in the surface area of HT. The HP highly influences the system's thermal performance, and its effective HT characteristics are more pronounced at lower HP levels.

## 1. Introduction

Heat sinks are a necessary component for the purpose of dissipating heat generated by energy-intensive devices and processes. HSs play a crucial role in the field of thermal management as they enhance the operational safety and cycle life of high-power density batteries [1,2]. The energy produced in fuel cells results from electrochemical reactions, with around 50% released as heat [3,4]. Similarly, the employment of single-phase forced convection in a highly supercooled HS has been

\* Corresponding author.

E-mail address: [ameer.a.jaddoa@uotechnology.edu.iq](mailto:ameer.a.jaddoa@uotechnology.edu.iq)

<https://doi.org/10.37934/arfmts.116.1.4063>

recognized as an effective method for chilling, offering a diverse range of applications [5]. In order to ensure the temperature of fuel cells remains within an acceptable range, it is necessary to employ an HS, despite the natural heat dispersion. Hence, the efficacy of HSs plays a crucial role in operating batteries, fuel cells, laser arrays, and electronic circuits. Further, HSs play a crucial role in the optimal functioning of electronic components, mainly due to the significant impact of temperature elevation on electronic failures, which accounts for approximately 55% of such occurrences [6,7]. The Nusselt number is unaffected by variations in HP when distilled water is employed as a coolant [8]. Nevertheless, the performance of TiO<sub>2</sub> nanofluid is enhanced at lower HP due to the increased stability of nanoparticles when combined with the base fluid under these conditions. As a result, the experiment demonstrated a significant improvement of 12.75% compared to distilled water when subjected to a HP of 100 W. According to the source provided by Jung and Park [9], The usage of nanofluid as the operational fluid in the Microchannel Heat Sink (MCHS) resulted in a thermal entropy generation rate that was 6.3% lower compared to water. In summary, our study involved the empirical demonstration of nanofluid HT by the utilisation of a technology for measuring velocity and temperature. The findings of this research will contribute to the advancement of the field of HT through the use of Al<sub>2</sub>O<sub>3</sub> nanofluids. The experimental results indicate that while utilizing nanofluids containing 0.012% TiO<sub>2</sub>, a heat sink (HS) with a wavelength of 5 mm and amplitude of 0.5 mm, operating at a Reynolds number of 894 and a heating power of 25 W, the minimum wall base temperature is measured to be 33.85 °C. Additionally, the maximum augmentation in Nusselt number is observed to be 40.57%. The power needed for pumping is determined by the flow rate and the pressure drop. The HS with a minimum wavelength is connected with a maximum value of 0.0284 W [10]. The thermal resistance (Rt) can be reduced by the heat conduction of liquid metal in the Z direction and the heat convection occurring between the top surface of the fins and the liquid metal. The aforementioned procedure demonstrated efficacy in microchannels characterized by a low channel aspect ratio, low mean velocity (Um), or lengthy heat sink length. The paper's example demonstrated a reduction in thermal resistance of up to 36.0%. The increased volume of space provided the heat sink with decreased pressure, perhaps resulting in a further reduction in pumping power (P). This condition was shown to be applicable in cases where the fins were shortened ( $h_2 < 0$ ;  $h_2$  represents the height of the expanded channel for E-MCHS) as well as when the cover plate was elevated ( $h_2 > 0$ ) [11]. The findings indicate that the utilization of a mini/micro-channel stacked double-layer HS can lead to a notable reduction in pressure drop when compared to the single-layer micro-channel heat sink configuration. The average convection HT index of the tiny-channel stacked double-layer HS is higher than that of the single-layer micro-channel HS when the flow rate ratio is less than 2.0. Ultimately, the FOM ratios exhibit values exceeding unity across all instances. According to the referenced study, the utilization of tiny-channel stacked double-layer HSs offers more benefits in engineering applications compared to single-layer tiny-channel HSs. The study conducted by Wang *et al.*, [12] proposed the integration of a multi-objective optimization algorithm with computational fluid dynamics (CFD) and machine learning techniques as a means to reduce the expenses associated with optimization and computational processes. The goal of the research was to identify the optimal operational parameters for mini-channel heat sinks utilizing nanofluids. Initially, a numerical model was constructed to simulate the behavior of a nanofluid mini-channel. The mixture model was employed to build a comprehensive dataset that could be utilized for training machine learning models. Here, we used the Support Vector Regression (SVR), Gaussian Process Regression (GPR), and Random Forest (RF) models to show how the variables of the nanofluid tiny-channel (namely the inlet Reynolds number (Re), volume fraction ( $\phi$ ), and heat flow density (q) relate to the pressure drop ( $\Delta P$ ) and the average temperature of the heating wall (Tave). The study showed that the Gaussian Process Regression (GPR) model was the most suitable. R<sup>2</sup> values of 0.9939 for Tave and 0.9985 for

P showed this. The NSGA-II multi-objective optimization method was used to find the best value for  $\phi$  in various operational situations. The findings revealed a value of around 3% for low Reynolds number (Re) and approximately 2% for high Reynolds number (Re). The user's content does not include any information to alter. This research examines how well various machine learning algorithms and a regression model can guess the complicated connections between geometric shapes and operational variables and how well heat moves through materials [13-15]. The machine learning models had mean absolute errors (MAEs) ranging from 7.5% to 10.9%. This showed a significant improvement in the accuracy of the predictions, about five times better than the current regression correlations. The model demonstrated significantly fewer mean absolute errors (MAEs) than the regression model. In addition, the machine learning models demonstrated a notable level of precision when applied to infrequent geometric shapes and specific operational circumstances, such as a triangle pin shape or the utilization of R134A as a working fluid [16-20]. The findings of this study demonstrate the higher predictive accuracy of machine learning models compared to traditional correlation methods in assessing the thermal performance of tiny-pin fin HSs across various geometry and operating situations. The age range of the individuals mentioned is between 15 and 17 years old. The evaluations presented herein serve the purpose of comprehending the physical mechanisms underlying microchannels across many application domains. Moreover, they aim to address the existing gaps in relevant research and offer valuable study methodologies for forthcoming numerical investigations. The user has provided a numerical reference without any accompanying text. The evaluation of the impact of the radius ratio on heat storage efficiency is also conducted in the absence of gravitational forces [21,22]. This study demonstrates the efficacy of electrohydrodynamics in facilitating the melting process of phase transition materials, even in microgravity conditions. The user provided a numerical reference without any accompanying text. The findings indicate that the utilization of MWCNT nanofluids in the microheat exchanger leads to a notable improvement in heat transfer efficiency, with an enhancement of up to 33%. Furthermore, the enhancement of the system's energy efficiency is observed under specific operating conditions, particularly in the vicinity of a Reynolds number (Re) of approximately 1000, considering HT results and pressure drop. Additionally, a proposed correlation is presented to assess the HT results of nanofluids in tiny-channels based on the average Nusselt number. The user has provided a numerical reference. The investigation of the characteristics of  $\text{Al}_2\text{O}_3$ - $\text{H}_2\text{O}$  nanofluid in minichannels involves the utilization of experiment comparison and numerical analytic techniques to evaluate irreversibility [23,24]. The experimental findings indicate that the critical transition point of the nanofluid, at which it transitions from laminar flow to turbulent flow, is determined to be 1300. The Nusselt number of the nanofluid consisting of  $\text{Al}_2\text{O}_3$  and  $\text{H}_2\text{O}$  exhibits the highest enhancement in concentration at 0.01% when the Reynolds number (Re) is approximately 5200, resulting in a maximum rise of 47.5%. The observed augmentation in the friction factor of the nanofluid amounts to 15.1% [25-29]. The findings of earlier experiments were compared to determine the effective heat transfer of low-concentration nanofluids under low flow resistance, as indicated by the Nu and f values. The primary source of irreversible loss in the nanofluid is the thermal entropy production rates, while the frictional entropy generation rate dominates prior to a Reynolds number of 5000.

This study addresses the enhancement of heat transmission in mini-channels through the utilization of nanosized particles of  $\text{TiO}_2$  nanofluid within the flow channel. In recent years, there has been a significant global focus on the investigation of nanomaterials and their dispersion in fluids as particles. This heightened interest can be attributed to the groundbreaking findings of pioneering researchers, who uncovered the abnormal thermal properties shown by these fluids. Heat transfer from smaller locations is accomplished by utilizing mini-channels. According to the theory of heat transfer, the most efficient heat transmission occurs in mini-channels when there is a little pressure

drop across them. This research study focuses on conducting experimental investigations to analyze the enhanced heat transfer properties of three different configuration models of tiny-channel HSs through the utilization of TiO<sub>2</sub> nanofluid. The comparative analysis involves the examination of experimental outcomes pertaining to heat transfer utilizing TiO<sub>2</sub> nanofluid, in relation to three distinct design models of the tiny-channel HS.

## **2. Experimental Methodology**

A test rig of an experimental nature was created and afterwards deployed within the Heat Transfer Laboratory, which is housed under the Mechanical Engineering Department of the University of Technology. The schematic representation of the equipment's overall configuration is depicted in Figure 1, while Figure 2 provides a photographic depiction of the same. The test rig was specifically developed to allow for the manipulation and experimentation of different operating parameters. The primary constituents of this units consist of experimental systems, a cooling fluid, measuring equipment, a reservoir, a power supply, and a cooling unit. Figure 3 illustrates the various modules of the heat sink with serpentine mini-channels. The cooling medium utilized in the system was distilled water. This fluid is introduced into the system from a reservoir, passing through a filter before traversing the heat sink. Within the heat sink, the coolant undergoes a temperature increase as it absorbs thermal energy from the heat source. It is imperative to ensure that the coolant is sufficiently cooled prior to its re-entry into the heat sink for the purpose of recirculation. The aforementioned procedure was executed employing a radiator cooler. Consequently, the heated coolant underwent a cooling process at the radiator cooler before being returned to the storage tank for continual recirculation through the system via a pump. The pump produces a sufficient level of energy to generate pressure, so enabling the circulation of the cooling fluid within the module. In a series of investigations, the manipulation of coolant flow rates was achieved by the utilization of a globe valve for control. The flow meter is employed to measure the volumetric flow rate within the closed-loop system. The heat source is situated on the underside of the SMCHS. The plate-type heater has a maximum heat input of 500 W when operated at a voltage of 230 V. The primary function of this device is to provide input heat to the SMCHS, while also offering the capability to regulate the heat output through the utilization of a variac. The instruments utilized for measuring electrical power consist of a voltmeter and an ammeter. The primary power source's alternating current (AC) voltage is reduced through the utilization of a stepdown transformer. As a result, the heat input applied to the bottom surface of the SMCHS remains constant for every test. A total of five perforations were strategically created along the center axis of the heat sink base, which consists of interconnected serpentine mini-channels. Following this, the thermocouples were carefully put into these perforations in order to precisely measure the temperatures of the base. The holes are uniformly spaced at a depth of 4mm below the mini-channel substrate. The measurement of the average bulk wall temperature is accomplished using K-type thermocouples equipped with 1mm beads. The temperature of the liquid coolant is monitored by the placement of two thermocouples, spaced 1.5 cm apart, at the intake and outflow points of the channel. Digital differential manometers are used to quantify the reduction in pressure of the submental chin-hold maneuver and swallow (SMCHS). The flow meter has been specifically designed for the purpose of monitoring volumetric flow rates of water, with a measurement range spanning from 1 to 10 liters per minute (Lpm). In order to enhance heat transmission and minimize the presence of air gaps, it is customary to apply a thermal compound to the heater and channel sink surfaces. Glass wool insulation is effective in minimizing heat loss inside the heater assembly channel. The power output of a variac was enhanced by maintaining a constant value, while the flow rate was managed by a stable control valve. The

experimental conditions were fixed for a duration of 30 minutes. A study was conducted to quantitatively analyze volume flow rates ranging from 1 to 6 Lpm, with an associated uncertainty of  $\pm 4\%$ . The heat load has a range spanning from 40 to 400 watts, accompanied by a 1% margin of error. The heat sink was maintained at a temperature below  $90\text{ }^{\circ}\text{C}$ , while the fluid entering the system was maintained at a temperature of  $27\text{ }^{\circ}\text{C}$ . The accuracy of pressure drop measurements is within a range of 1%.

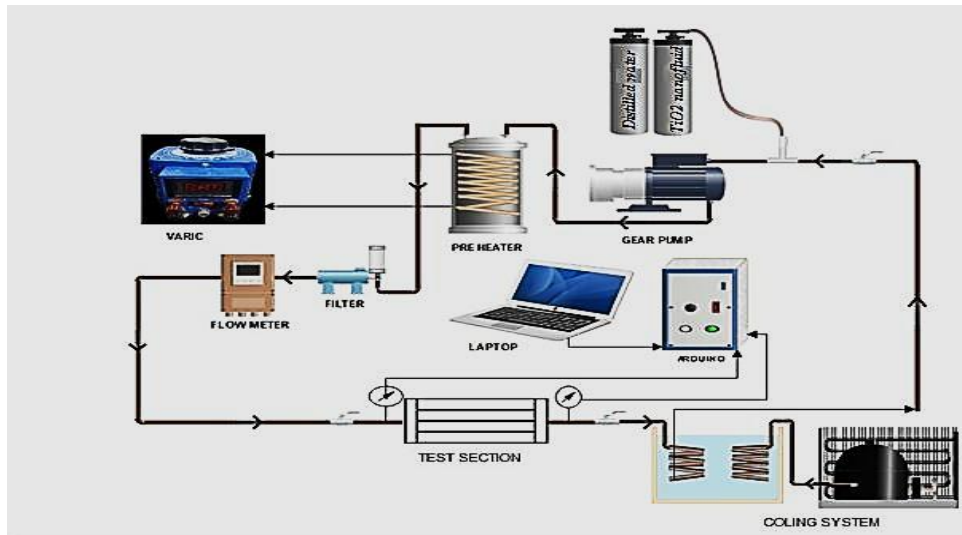
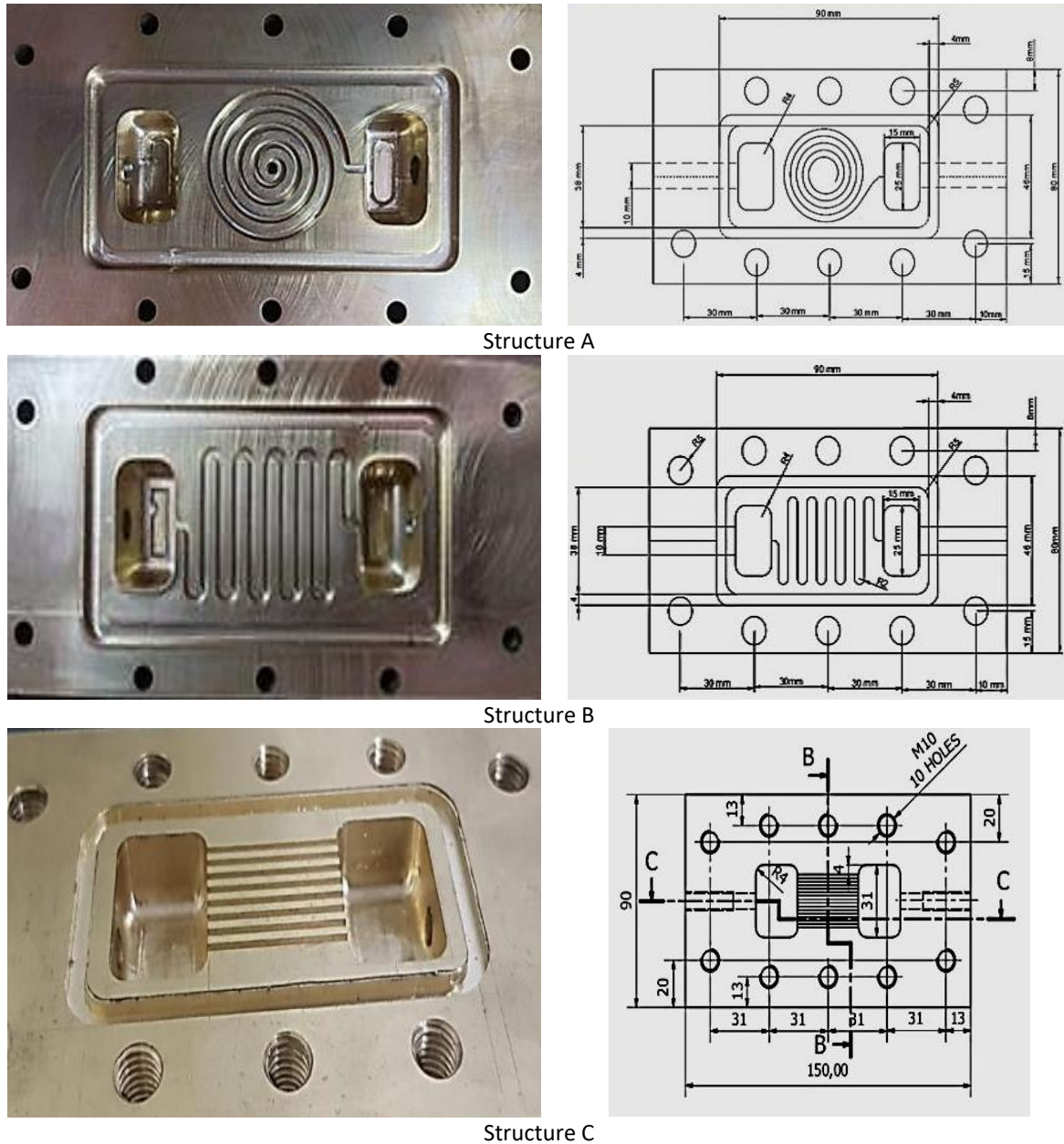


Fig. 1. Graph represents the experimental model



Fig. 2. Graph illustrates the empirical model



**Fig. 3.** The configurations of all serpentine mini-channels heat sink

The Rutile form of  $\text{TiO}_2$  nanofluid, which was utilized in this study, was procured from Nanoamor, a supplier based in Malaysia. The nanoparticles were not stabilized using a surfactant, and a homogenous dispersion of  $\text{TiO}_2$  nanoparticles was created by changing the pH and bead-milling, using pure water. The manufacturer provided information regarding the size and morphology of the nanoparticles, stating that they ranged from 5 to 30 nm in size and had a spherical shape. In addition, it is worth noting that the nanofluid under investigation was not subjected to sonication prior to experimentation. This decision was based on the fact that the nanofluid exhibited a stable state for a duration of six months at room temperature, as depicted in Figure 4.



Fig. 4. TiO<sub>2</sub> nanofluid

### 3. Data Reduction

The volume fraction ( $\alpha$ ) of nanofluid can be calculated using Eq. (1) based on the provided weight fraction of nanoparticles [8].

$$\alpha = \rho_{bf} W_{np} \times (\rho_{np} - \rho_{np} W_{np} + W_{np} \rho_{bf})^{-1} \quad (1)$$

The density of the nanofluid is a function of both the density of the nanoparticles and the base fluid. For the purpose of determining the density of nanofluid, the following Eq. (2) is utilized

$$\rho_{nf} = \alpha \rho_{np} + \rho_{bf} - \alpha \rho_{bf} \quad (2)$$

The density of the nanofluid as well as the specific heat capacity of the base fluid both play a role in determining the specific heat capacity of the nanofluid. It is determined by using the following equation, Eq. (3) [8]

$$c_{pnf} = (\alpha \rho_{np} c_{pnp} + \rho_{bf} - \alpha \rho_{bf} c_{pbf} + \rho_{bf} c_{pbf}) \times \rho_{bf}^{-1} \quad (3)$$

Viscosity of the suggested model for a nanofluid, taking into consideration the size of nanoparticles, is provided as Eq. (4)

$$\mu_{nf} = \mu_{bf} [1 - \alpha^{1.03} \times (d_{np} d_{pf}^{-1})^{-0.3}] \quad (4)$$

And  $d_{pf}$  can be calculated as in Eq. (5)

$$d_{pf} = 0.1 [6M \times (\pi N \rho_{bf})^{-1}]^{1.333} \quad (5)$$

where molecular weight of water,  $M = 18$  g/mole, Avogadro no.,  $N = 6.02 \times 10^{23}$  and  $\pi = 3.14$ .

Eq. (6) obtained the computation of the thermal conductivity of nanofluids (6)

$$k_{nf} = (k_{bf}k_{nf} + 2k_{bf} - s2k_{bf} - 2k_{bf}s k_{nf}\alpha - k_{bf}k_{nf}\alpha) \times (k_{bf}k_{nf} - 2k_{bf}k_{nf} + 2k_{bf}\alpha - k_{bf}k_{nf}\alpha)^{-1} \quad (6)$$

where,  $s = 3$  for spherical shape nanoparticle.

Heat is transferred from the heat sink to the coolant whenever there is motion involved. The rate of heat transmission can be determined by applying Eq. (7) to the situation

$$Q = m \cdot c_p T_{out} - m \cdot c_p T_{in} \quad (7)$$

The mean temperature of the bulk coolant is used in the calculation of all thermophysical properties, which is done by using the following equation

$$T_m = 0.5T_{in} + 0.5T_{out} \quad (8)$$

The temperature at the base is measured at a depth of 1.5 mm below the surface of the channel wall. The temperature can be determined using Fourier's equation of heat conduction, as expressed in Eq. (9).

$$T_{wl} = T_{tc} - QH_w \times (K_{hs} W_t L_t)^{-1} \quad (9)$$

The calculation of the heat transfer rate, expressed in terms of the convective heat transfer coefficient, is determined using Eq. (10).

$$Q = (LMTD)(htw_c L_t + h2th_f L_t) \quad (10)$$

where total number of channels,  $t = 17$ .

The LMTD (Logarithmic Mean Temperature Difference) represents the average temperature difference between the wall and the mean bulk temperature of the coolant. The calculation can be performed using Eq. (11).

$$LMTD = [(T_{wl} - T_{in}) - (T_{wl} - T_{out})] \times \ln [(T_{wl} - T_{out}) \times T_{wl} - T_{out}^{-1}]^{-1} \quad (11)$$

Convective heat transfer coefficient is calculated by Eq. (12)

$$h = m \cdot C_p (T_{out} - T_{in}) \times (A_e LMTD)^{-1} \quad (12)$$

The evaluation of integral-fin efficiency, as stated by the equation, relies on the consideration of convective thermal resistance as a significant parameter (13)

$$R_{th} = LMTD \times A_c \times Q^{-1} \quad (13)$$

Reynolds number is obtained by Eq. (14)

$$Re = \rho \times \left(\frac{4A_c}{P_c}\right) \times \left(\frac{Q_f}{W_{chf}}\right) \times \mu^{-1} \quad (14)$$

The heat transfer performance, as measured by the experimental Nusselt number, is mathematically described by Eq. (15).

$$Nu = h \times k^{-1} \times \left(\frac{4A_C}{P_C}\right) \tag{15}$$

This experimental Nusselt number is compared with the empirical correlation given by Peng and Peterson [21], Eq. (16)

$$Nu = Re^{0.62} \times Pr^{0.3} \times \left(\frac{d_h}{w_{cc}}\right)^{0.81} \times \left(\frac{h_f}{w_{cc}}\right)^{-0.79} \times 0.11 \tag{16}$$

#### 4. Uncertainty Analysis

The approach used to determine the uncertainty associated with experimental data is the Kline and McClintock's [22] method. The log mean temperature difference and Nusselt number exhibit a maximum uncertainty of 3.25% and 6.87% respectively.

#### 5. Interpretation of the Results

##### 5.1 Model Verification

In the first stage, the experimental results are compared with the theoretical correlation proposed by Peng and Peterson [21], using distilled water as the medium. As depicted in Figure 5, the experimental Nusselt number exhibits minimal sensitivity to the augmentation of heating power from 100W to 300W. The observed pattern exhibits a consistent incremental trend as the Reynolds Number increases. The experimental Nusselt number is shown to be in agreement with the theoretical correlation within a margin of error of 12% across all heating powers, therefore validating the results.

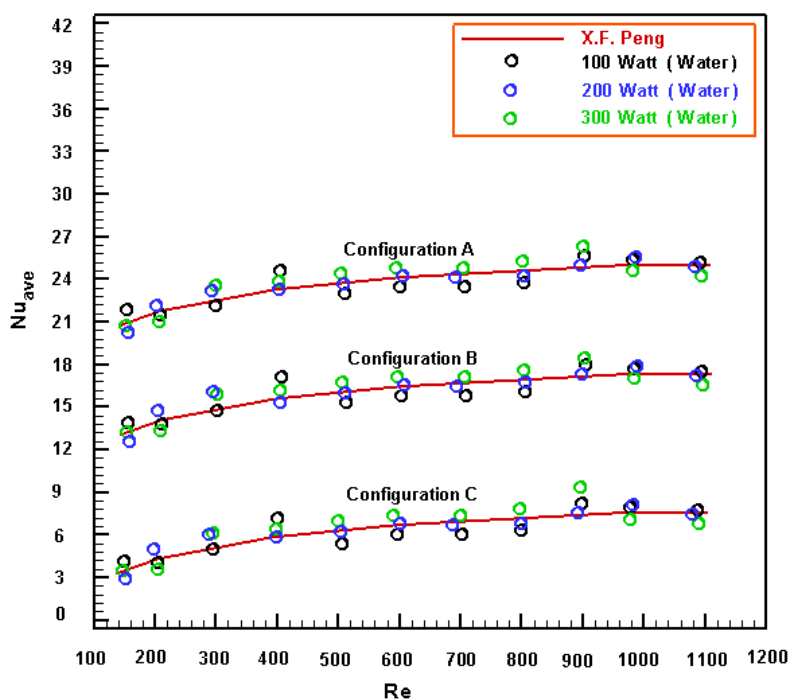
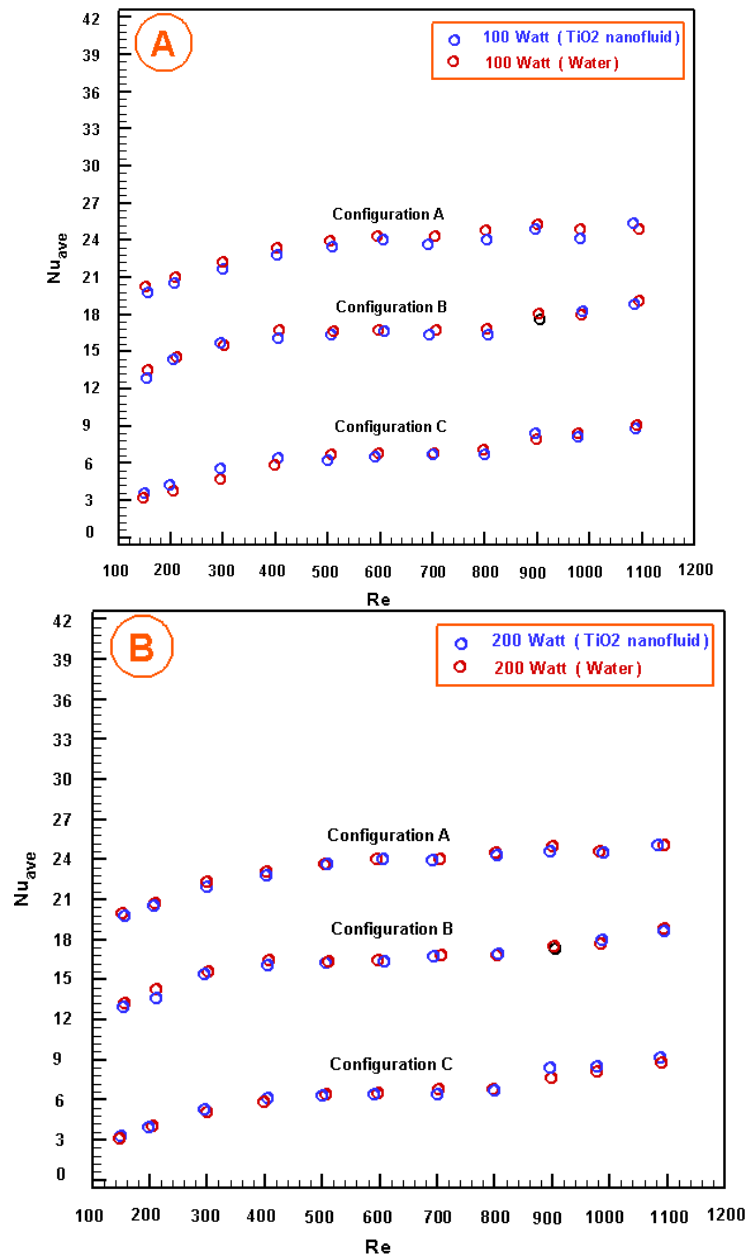


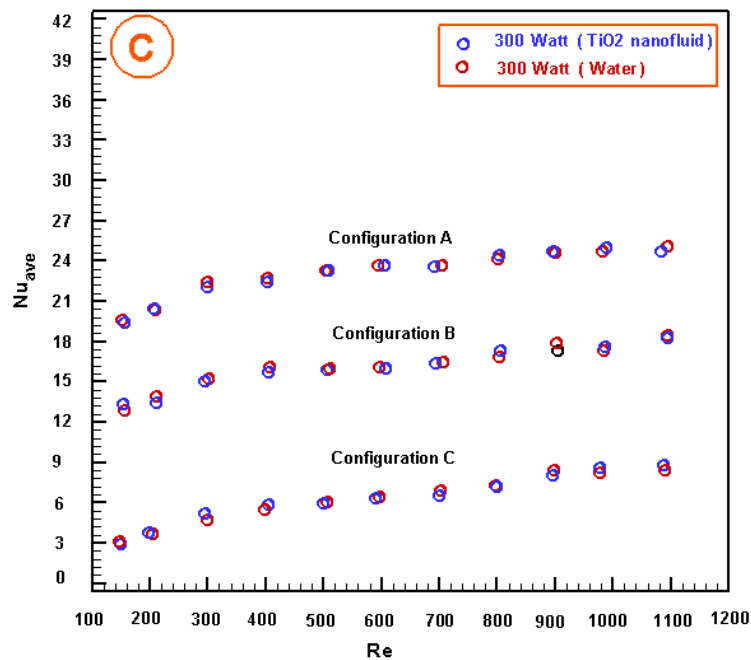
Fig. 5. Graph represents the Nusselt number, Peng and Peterson [21] and Kline and McClintock [22] comparison

## 5.2 TiO<sub>2</sub> Nanofluid against Distilled Water, Performance Analysis

### 5.2.1 Nusselt number

The Nusselt number has a positive correlation with the Reynolds number when considering both distilled water and TiO<sub>2</sub> nanofluid across various HPs. The Nusselt number associated with TiO<sub>2</sub> nanofluid exhibits a greater value in comparison to that of distilled water. Nevertheless, the rate of promotion is decreasing as the heating power increases, as depicted in Figure 6(a) to Figure 6(c). As a result, the highest level of improvement seen at 100W is 11.32%. However, the level of enhancement decreases to 2.46% and 1.82% for heating powers of 200W and 300W, respectively.

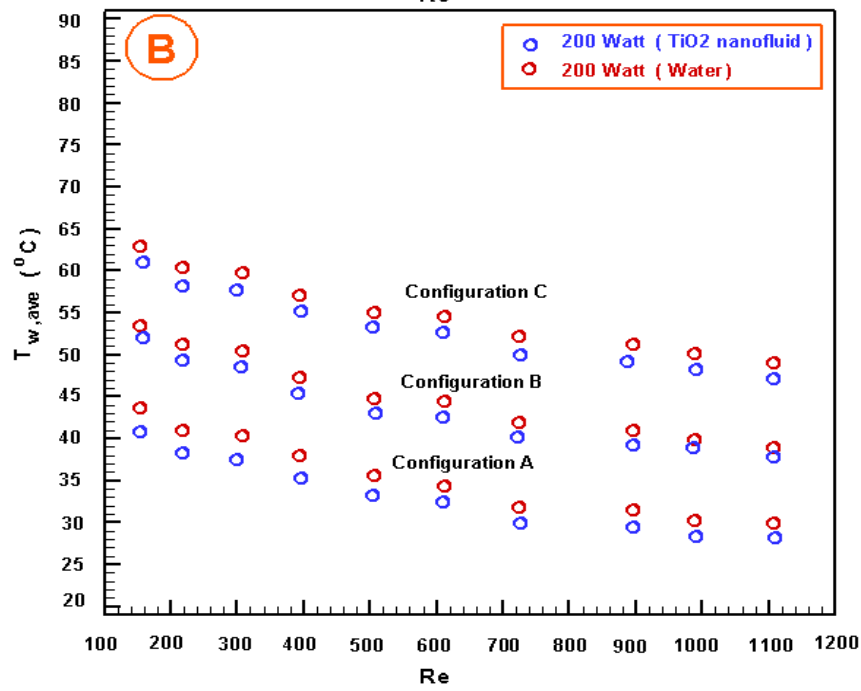
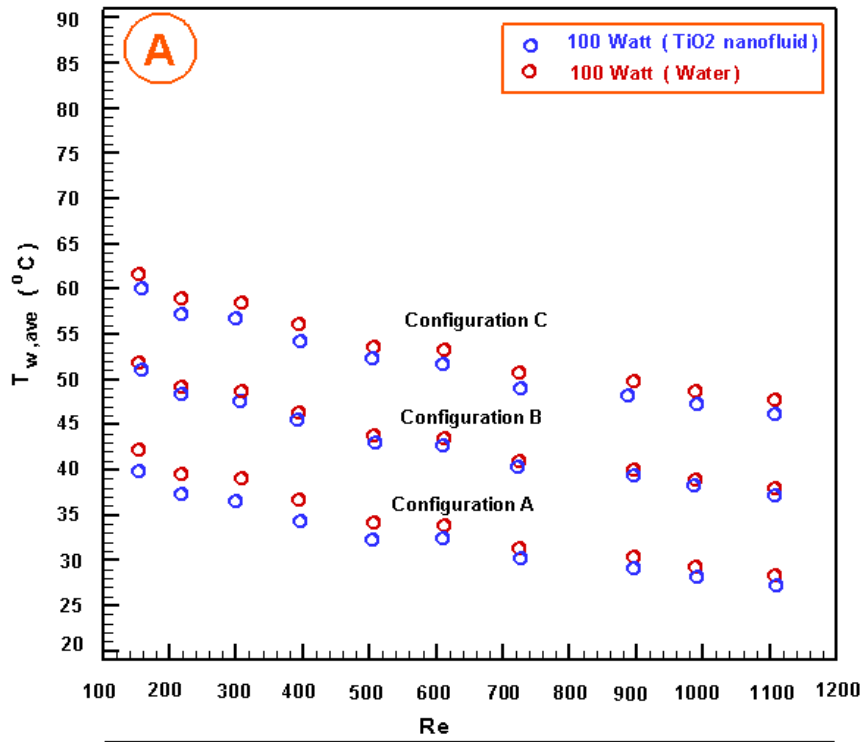




**Fig. 6.** TiO<sub>2</sub> nanofluid against distilled water, graphic as a function of Nusselt number and Reynolds number

### 5.2.2 Temperature of the innermost wall

The Nusselt number of TiO<sub>2</sub> nanofluid is greater than that of pure water. This observation suggests that the rate of reduction in the inner wall temperature of the small channel HS is higher when TiO<sub>2</sub> nanofluid is used compared to when distilled water is used, as seen in Figure 7(a) to Figure 7(c). On the contrary, previous studies have shown that the use of TiO<sub>2</sub> nanofluid has a greater efficacy in reducing wall temperature when subjected to lower HP settings as opposed to higher HP conditions. The aforementioned findings demonstrate that when subjected to heating powers of 100 W, 200 W, and 300 W, the temperature of the inner wall exhibited a reduction of 3.83%, 3.62%, and 3.56% correspondingly. In the experimental investigation conducted, a TiO<sub>2</sub> nanofluid was used at a Reynolds number of 1100, corresponding to a HP of 100 W. The lowest temperature of the wall was determined to be 55.35°C by measurements.



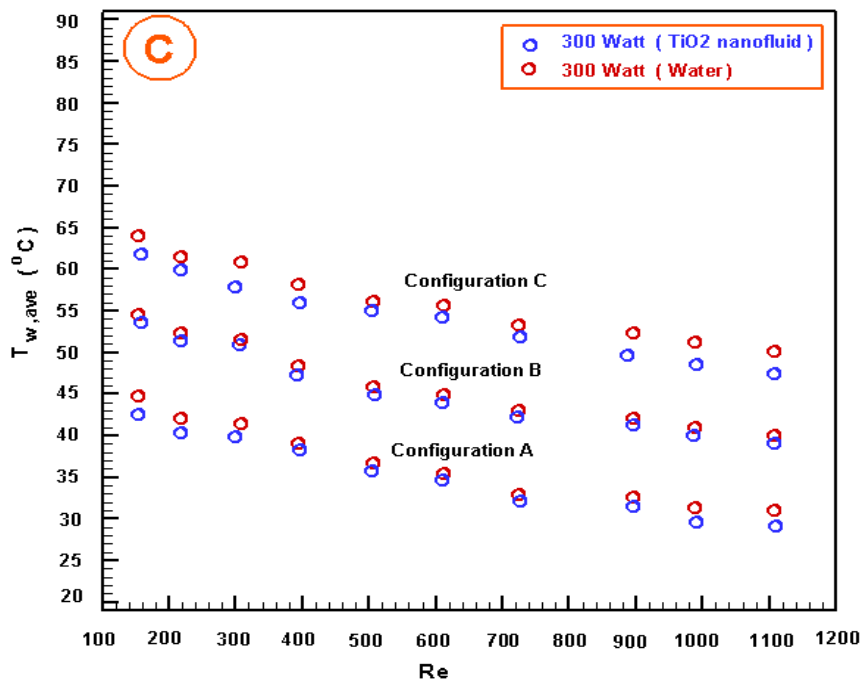
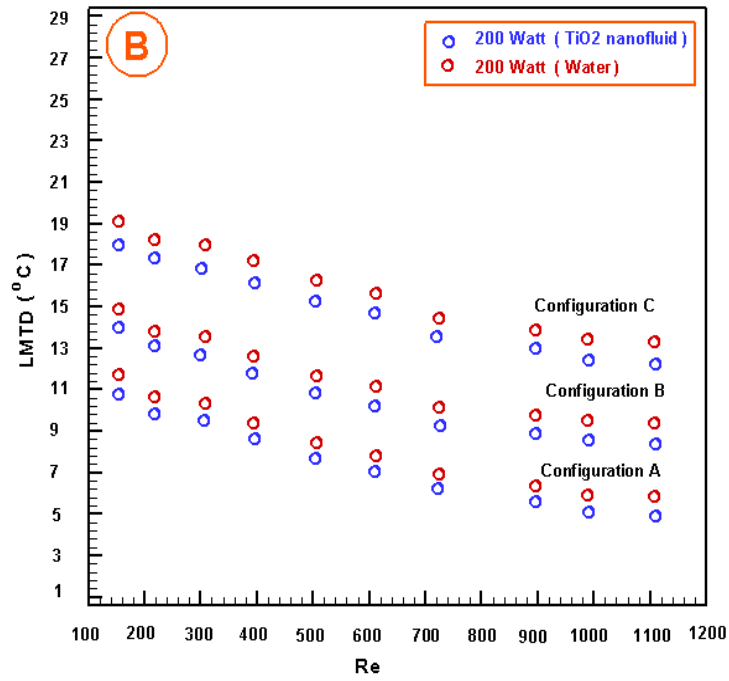
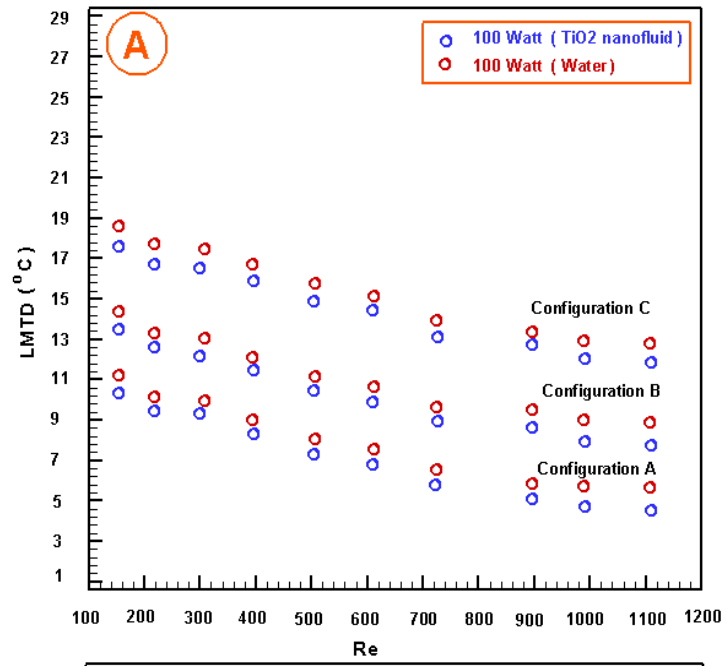
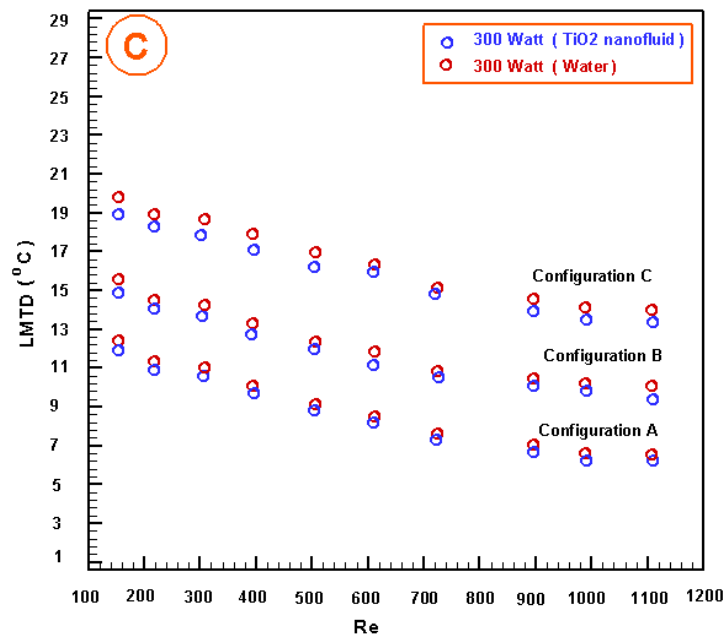


Fig. 7. Plotting innermost wall heat degree vs. Reynolds value compare TiO<sub>2</sub> nano-fluid with clear water

### 5.2.3 Log mean temperature difference

The Logarithmic Mean Temperature Difference (LMTD) is a metric that quantifies the average disparity between the highest temperature of the inner wall of a tiny-channel HS and the temperature of the surrounding bulk coolant. The experimental results indicate that the TiO<sub>2</sub> nanofluid exhibits a lower wall temperature compared to distilled water, which can be attributed to its higher heat absorbing ability. This leads to a significantly reduced logarithmic mean temperature difference (LMTD) for the TiO<sub>2</sub> nanofluid across all heating power levels, as depicted in Figure 8(a) to Figure 8(c). Similar to the behavior observed in wall temperature, a more substantial decrease is observed when the heating output is reduced to 100 W. In general, the decrease rates associated with HPs of 100 W, 200 W, and 300 W are 19.35%, 13.67%, and 11.99%, respectively.

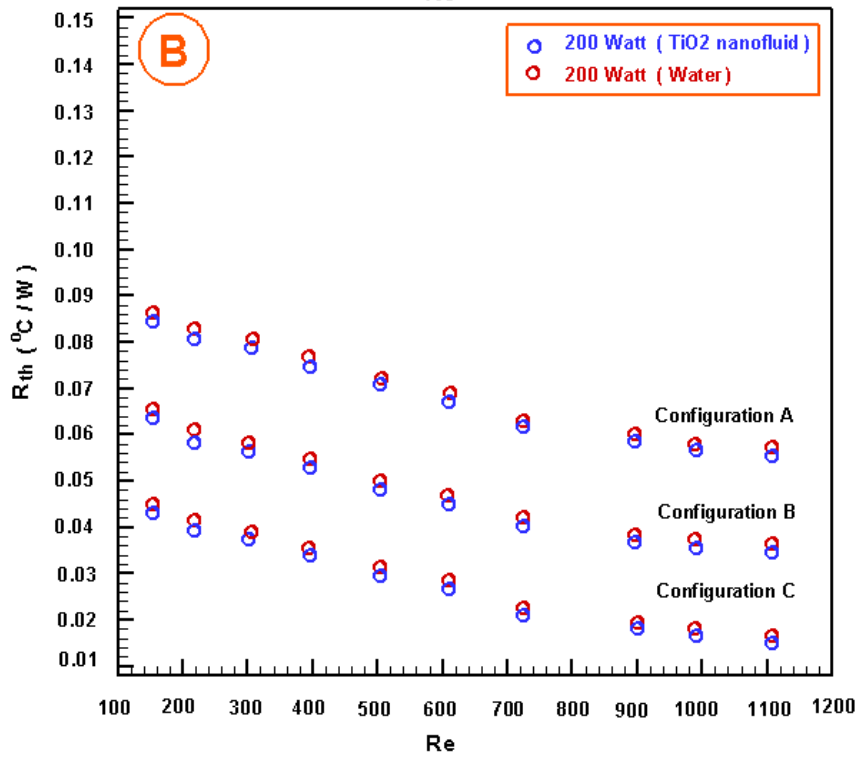
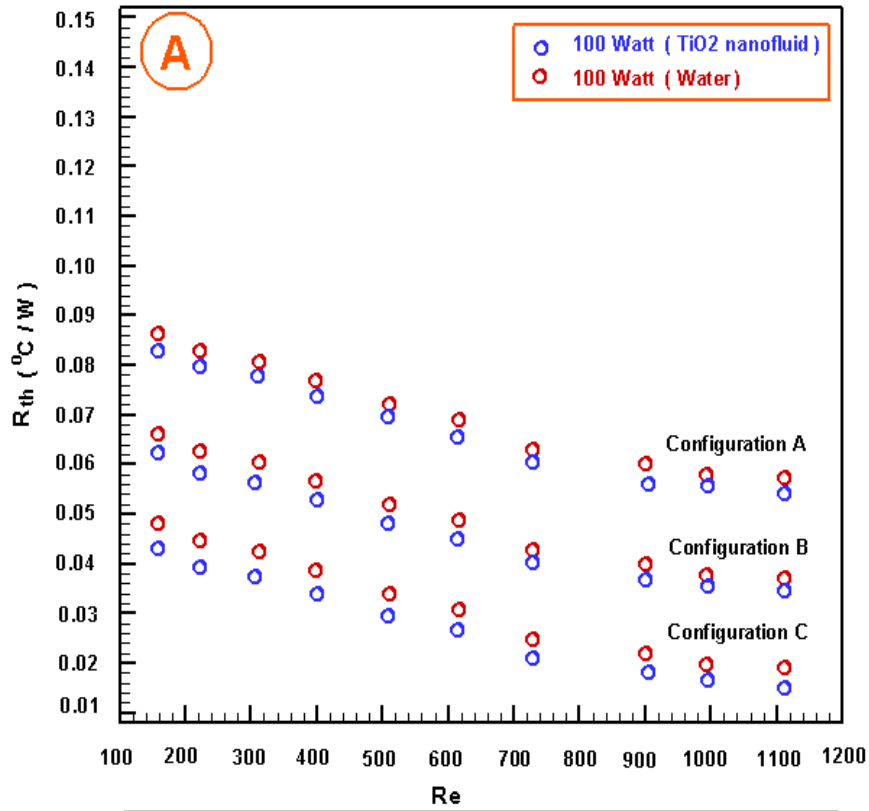


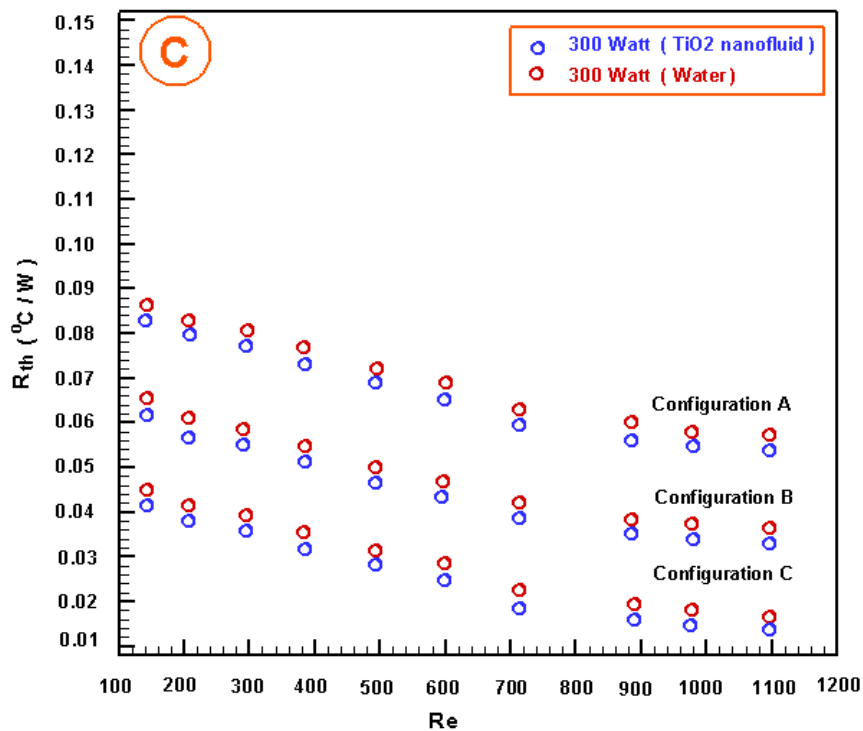


**Fig. 8.** TiO<sub>2</sub> nanofluid and distilled water are compared, and the results are displayed as log mean temperature difference against Reynolds number

#### 5.2.4 Thermal resistance (*R<sub>th</sub>*)

The fundamental indexes that demonstrates the behaviour of a minichannel HS is thermal resistance. A lower thermal resistance signifies superior heat sink performance, since it represents the ratio between the logarithmic mean temperature difference (LMTD) and the rate of HT. Figure 9(a) to Figure 9(c) illustrates the thermal resistance of distilled water and TiO<sub>2</sub> nanofluid, demonstrating a decrease in thermal resistance as the Reynolds number increments for both fluids. In addition, the utilization of TiO<sub>2</sub> nanofluid as a cooling medium result in a decreased thermal resistance compared to distilled water. Specifically, the reduction in thermal resistance amounts to 21.85%, 13.42%, and 10.23% for heating powers of 100 W, 200 W, and 300 W, respectively. The minimum thermal resistance observed in this study was found to be 0.064 OC/W. This result was obtained by utilizing a TiO<sub>2</sub> nanofluid at a Reynolds number of 1100, which corresponds to a HP of 100 W.

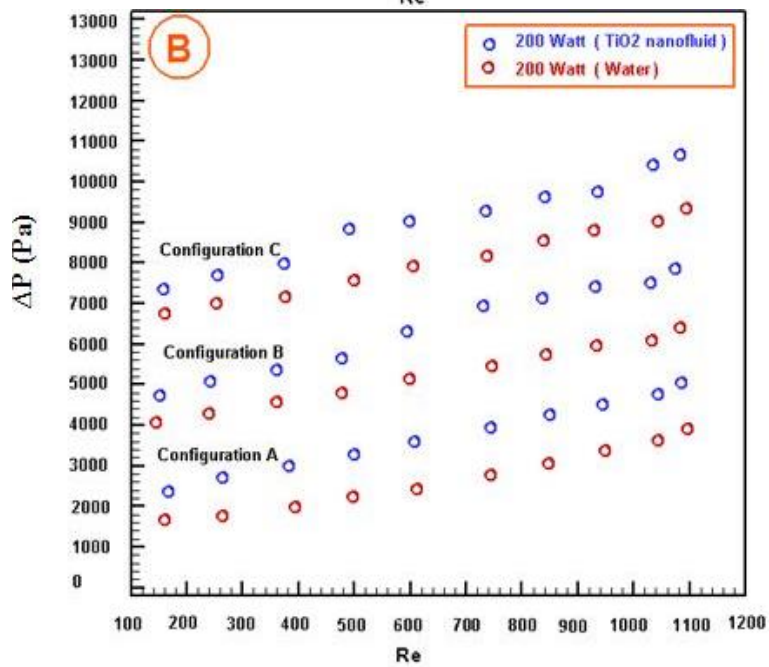
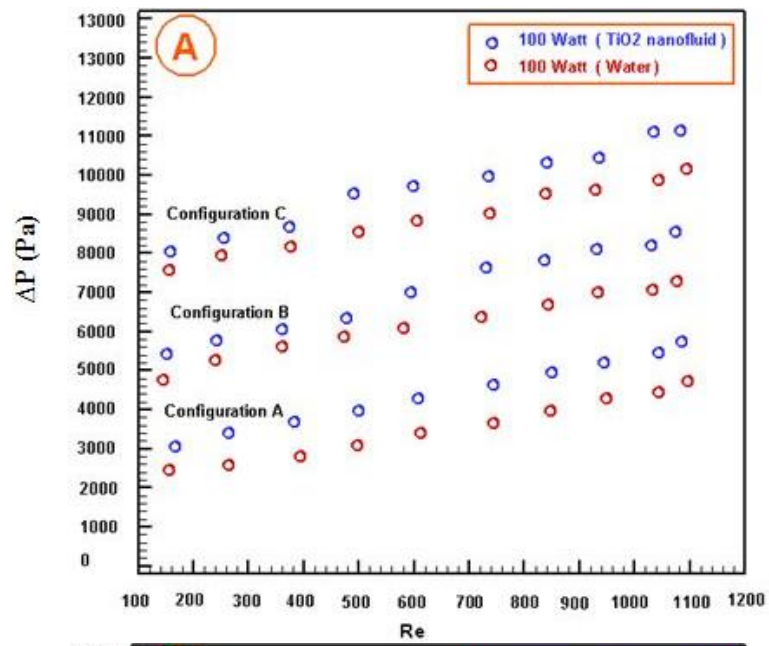


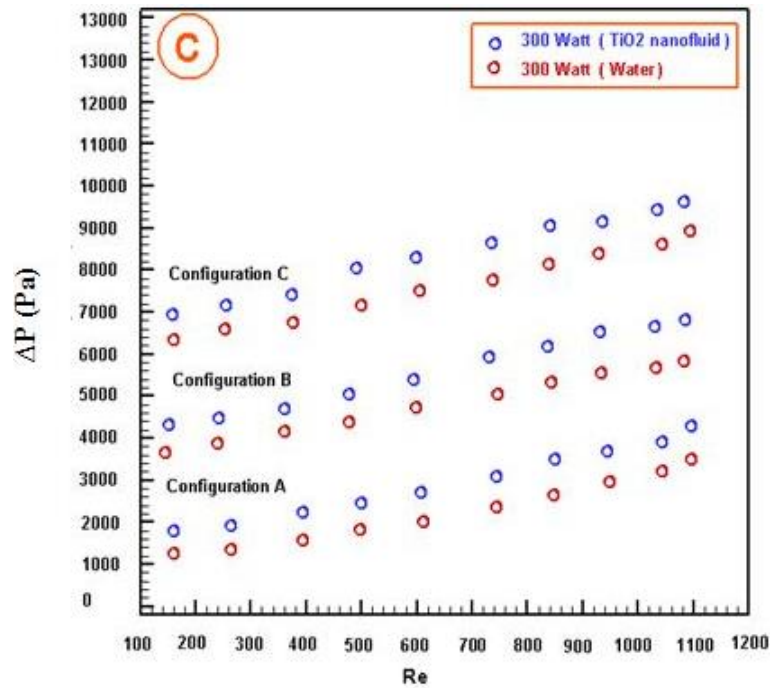


**Fig. 9.** Graph represents a comparison of TiO<sub>2</sub> nanofluid with distilled water,  $R_{th}$  against  $Re$

### 5.2.5 Pressure drop

The behaviour of a tiny-channel HS is primarily characterized by its thermal resistance, which serves as a fundamental parameter. Superior heat sink performance is shown by a lower thermal resistance, since it reflects the relationship between the logarithmic mean temperature difference (LMTD) and the heat transfer rate. Figure 10(a) to Figure 10(c) depicts the thermal resistance characteristics of distilled water and TiO<sub>2</sub> nanofluid, revealing a reduction in thermal resistance with increasing Reynolds number for both fluids. Furthermore, the implementation of TiO<sub>2</sub> nanofluid as a coolant result in a reduction in thermal resistance when compared to the use of distilled water. The thermal resistance is reduced by 21.85%, 13.42%, and 10.23% for heating outputs of 100 W, 200 W, and 300 W, respectively. The investigation revealed a minimal thermal resistance of 0.064 OC/W. The aforementioned outcome was achieved through the utilization of a TiO<sub>2</sub> nanofluid at a  $Re$  of 1100, which is representative of a HP of 100 W.

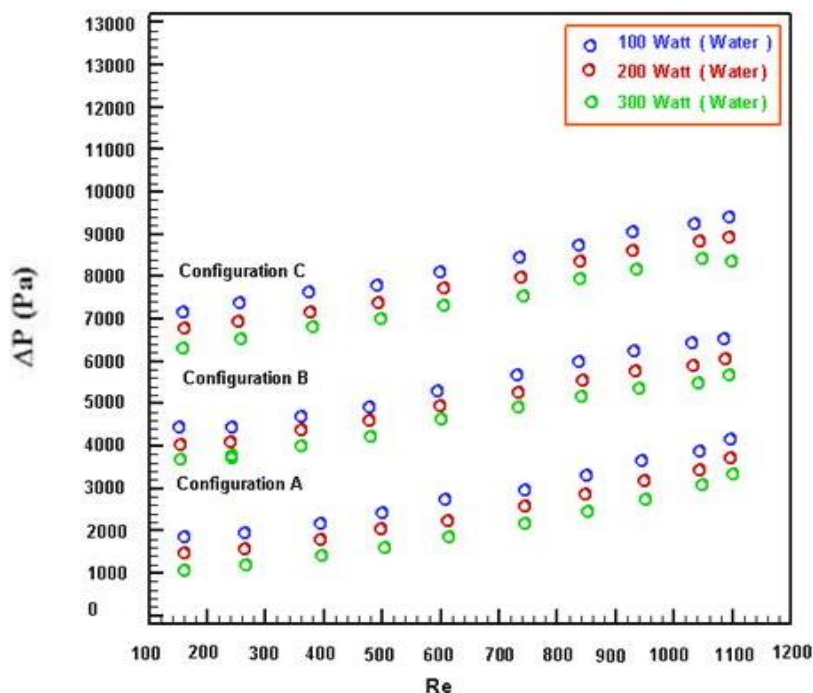




**Fig. 10.** Graph represents a comparison of TiO<sub>2</sub> nanofluid with distilled water, pressure drop against Re

### 5.2.6 Influences of heating power

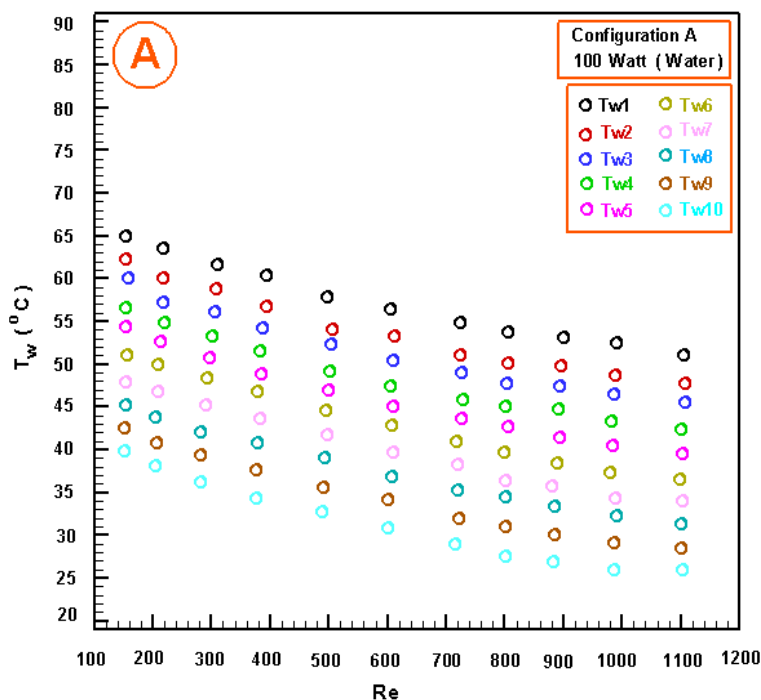
The analysis of the impact of HP on pressure decline is conducted employing pure water, as depicted in Figure 11. An increment in HP is relevant with a decrease in pressure drop. This phenomenon occurs due to a reduction in the density of the fluid as the heating power is raised. In general, a decrease of 13.24% in pressure drop is observed when comparing a HP of 200 W to a HP of 100 W. The significance of this particular form of pressure drop is highly relevant in the investigation of small channel heat sinks, as the determination of pumping power required is contingent upon the measurement of pressure drop.



**Fig. 11.** Heating influence on pressure decline, depicted as pressure decline against Reynolds number

### 5.2.7 Local base temperature

The measurement of local base temperature is a crucial factor in evaluating the effectiveness of coolant in maintaining optimal performance across the whole heat sink. As the coolant flows through the channel, it undergoes heat absorption, resulting in a gradual increase in local temperature from the input to the outlet. As a result, the efficiency of heat absorption by the coolant decreases as it progresses towards the outlet. The axial rise of the base temperature of the heat sink is illustrated in Figure 12(a) to Figure 12(c).



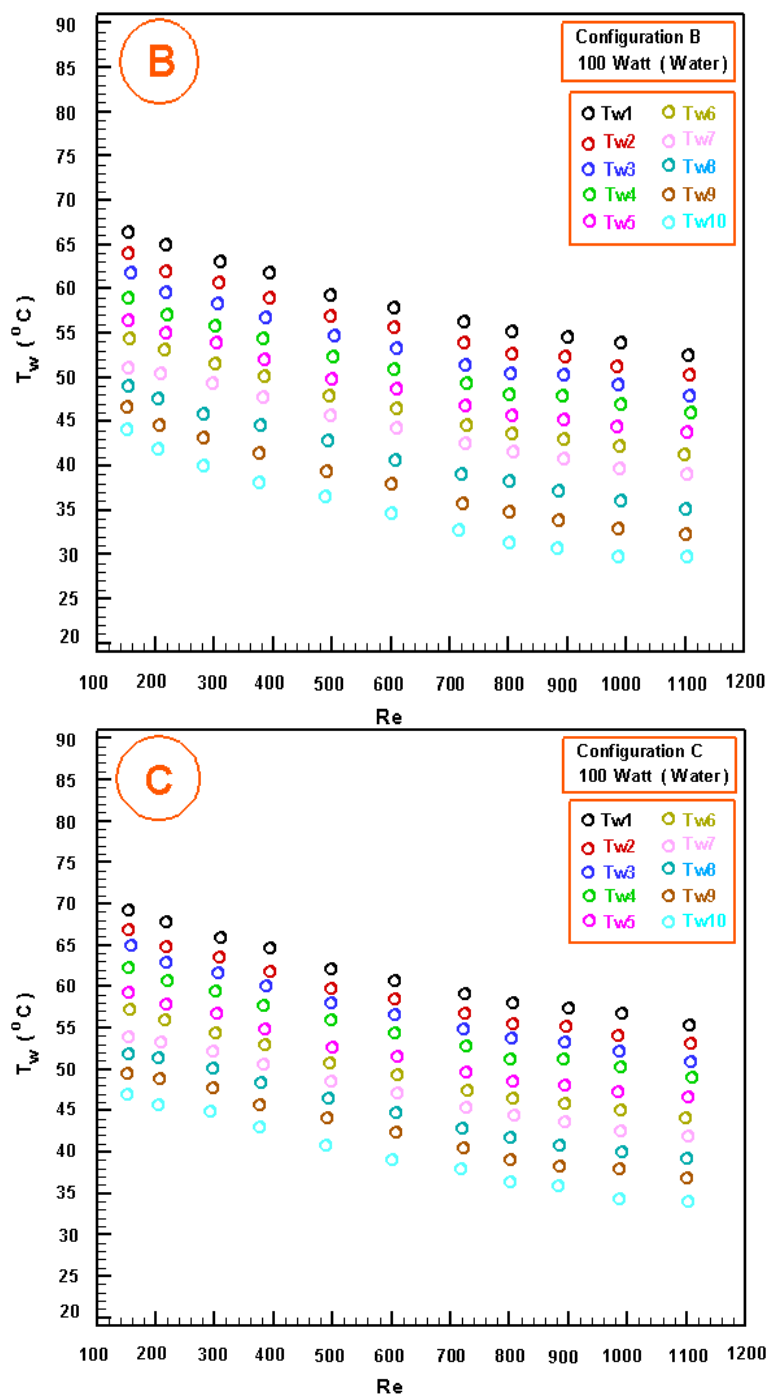


**Fig. 12.** Local base temperature, depicted in terms of temperature against Reynolds number

### 5.2.8 Ratio modification

The thermal enhancement of TiO<sub>2</sub> nanofluid, in comparison to distilled water, is illustrated in Figure 13. The findings suggest that the thermal performance of TiO<sub>2</sub> nanofluid is significantly influenced by the level of heating power, with more efficient heat transfer characteristics observed at lower heating power levels. As a result, Configuration A demonstrates a maximum enhancement of 19.59% for a heating power of 100W. However, the enhancement decreases to 12.64% and 7.34% for heating powers of 200W and 300W, respectively. The enhancement of Configuration B decreases to 8.15%, 6.83%, and 2.54% when the heating power is set to 100W, 200W, and 300W, respectively.

The enhancement of Configuration C decreases to 5.34%, 3.67%, and 1.21% when the heating power is set to 100W, 200W, and 300W, respectively.

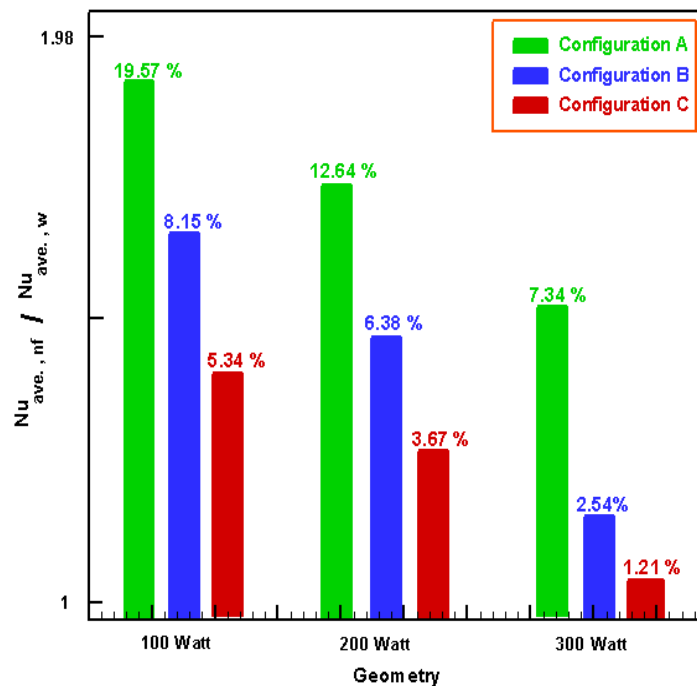


**Fig. 13.** Graph represents a comparison of TiO<sub>2</sub> nanofluid with distilled water, depicted as Nusselt number ratio against HP

## 6. Conclusion

This study examined the HT and pressure drop properties of distilled water and TiO<sub>2</sub> nanofluid in three different minichannel configurations with a hydraulic diameter of 1.2 mm. The investigation is conducted at HPs of 100 W, 200 W, and 300 W. The study of experimental outcomes yields several significant conclusions and can be concluded as follows. The Nusselt number remained unaffected by variations in HP when distilled water was employed as a coolant. Further, the performance of TiO<sub>2</sub> nanofluid is enhanced at reduced HP due to the increased stability of nanoparticles when combined with the base fluid. As a result, there has been a significant increase of 19.59% regarding Configuration A, specifically pertaining to the utilization of distilled water with a HP of 100 W. The increase of Configuration B decreases to 8.15%, 6.83%, and 2.54% for heating powers of 100W, 200W, and 300W, respectively. The enhancement of Configuration C decreased to 5.34%, 3.67%, and 1.21% when the HP was set to 100W, 200W, and 300W, respectively. An increase in the base temperature was noticed when TiO<sub>2</sub> nanofluid was circulated throughout the length of the heat sink. This phenomenon can be attributed to a reduction in the specific heat of the nanofluid. The minimum wall temperature was recorded as 40°C when employing TiO<sub>2</sub> nanofluid at a Reynolds number of 1100, corresponding to a heating power of 100 W. Ultimately, as the HP increases, there is a corresponding decrease in the pressure drop across the channels. This phenomenon occurred due to a reduction in the fluid density as the heating power was raised. Consequently, an increment in pressure decline of 12.34% is seen while utilizing distilled water at a heating power of 100W compared to a HP of 300W.

## References

- [1] Rao, Zhonghao, Qingchao Wang, and Congliang Huang. "Investigation of the thermal performance of phase change material/mini-channel coupled battery thermal management system." *Applied Energy* 164 (2016): 659-669. <https://doi.org/10.1016/j.apenergy.2015.12.021>
- [2] Huo, Yutao, Zhonghao Rao, Xinjian Liu, and Jiateng Zhao. "Investigation of power battery thermal management by using mini-channel cold plate." *Energy Conversion and Management* 89 (2015): 387-395. <https://doi.org/10.1016/j.enconman.2014.10.015>
- [3] Al-Tae'y, Kays A., Ameer Abed Jaddoa, and Hussain Saad Abd. "A loop thermosyphon for liquid cooled minichannels heat sink with pulsate surface heat flux." *Journal of Thermal Engineering* 7, no. 4 (2021): 1030-1038. <https://doi.org/10.18186/thermal.931389>
- [4] Ju, Hyunghul, Hua Meng, and Chao-Yang Wang. "A single-phase, non-isothermal model for PEM fuel cells." *International Journal of Heat and Mass Transfer* 48, no. 7 (2005): 1303-1315. <https://doi.org/10.1016/j.ijheatmasstransfer.2004.10.004>
- [5] Jaddoa, Ameer, Karema Hamad, and Arshad Hameed. "Fluid inflow and heat transfer enhancement: an experimental analysis of nanofluids in minichannel." *Frontiers in Heat and Mass Transfer (FHMT)* 20 (2023). <https://doi.org/10.5098/hmt.20.18>
- [6] Zhao, Jiateng, Zhonghao Rao, and Yimin Li. "Thermal performance of mini-channel liquid cooled cylinder based battery thermal management for cylindrical lithium-ion power battery." *Energy Conversion and Management* 103 (2015): 157-165. <https://doi.org/10.1016/j.enconman.2015.06.056>
- [7] Jaddoa, Ameer Abed. "Experimental investigation of supercritical fluid heat transfer properties in a miniature heat sink." *Journal of Mechanical Engineering (JMEchE)* 19, no. 2 (2022): 41-64. <https://doi.org/10.24191/jmeche.v19i2.19671>
- [8] Arshad, Waqas, and Hafiz Muhammad Ali. "Experimental investigation of heat transfer and pressure drop in a straight minichannel heat sink using TiO<sub>2</sub> nanofluid." *International Journal of Heat and Mass Transfer* 110 (2017): 248-256. <https://doi.org/10.1016/j.ijheatmasstransfer.2017.03.032>
- [9] Jung, Sung Yong, and Hanwook Park. "Experimental investigation of heat transfer of Al<sub>2</sub>O<sub>3</sub> nanofluid in a microchannel heat sink." *International Journal of Heat and Mass Transfer* 179 (2021): 121729. <https://doi.org/10.1016/j.ijheatmasstransfer.2021.121729>
- [10] Sajid, Muhammad Usman, Hafiz Muhammad Ali, Abu Sufyan, Danial Rashid, Saad Ullah Zahid, and Wajih Ur Rehman. "Experimental investigation of TiO<sub>2</sub>-water nanofluid flow and heat transfer inside wavy mini-channel heat sinks." *Journal of Thermal Analysis and Calorimetry* 137, no. 4 (2019): 1279-1294. <https://doi.org/10.1007/s10973-019-08043-9>
- [11] Zhang, Mingkuan, Xudong Zhang, Luna Guo, Xuan Li, and Wei Rao. "Flow and thermal modeling of liquid metal in expanded microchannel heat sink." *Frontiers in Energy* 17, no. 6 (2023): 796-810. <https://doi.org/10.1007/s11708-023-0877-5>
- [12] Wang, Qifan, Shengqi Zhang, Yu Zhang, Jiahong Fu, and Zhentao Liu. "Enhancing performance of nanofluid mini-channel heat sinks through machine learning and multi-objective optimization of operating parameters." *International Journal of Heat and Mass Transfer* 210 (2023): 124204. <https://doi.org/10.1016/j.ijheatmasstransfer.2023.124204>
- [13] Kim, Kiwan, Haeun Lee, Minsoo Kang, Geonhee Lee, Kiwook Jung, Chirag R. Kharangate, Mehdi Asheghi, Kenneth E. Goodson, and Hyoungsoon Lee. "A machine learning approach for predicting heat transfer characteristics in micro-pin fin heat sinks." *International Journal of Heat and Mass Transfer* 194 (2022): 123087. <https://doi.org/10.1016/j.ijheatmasstransfer.2022.123087>
- [14] Gao, Jie, Zhuohuan Hu, Qiguo Yang, Xing Liang, and Hongwei Wu. "Fluid flow and heat transfer in microchannel heat sinks: Modelling review and recent progress." *Thermal Science and Engineering Progress* 29 (2022): 101203. <https://doi.org/10.1016/j.tsep.2022.101203>
- [15] Sadique, Hussam, Qasim Murtaza, and Samsher Samsher. "Heat transfer augmentation in microchannel heat sink using secondary flows: A review." *International Journal of Heat and Mass Transfer* 194 (2022): 123063. <https://doi.org/10.1016/j.ijheatmasstransfer.2022.123063>
- [16] Deng, Daxiang, Long Zeng, and Wei Sun. "A review on flow boiling enhancement and fabrication of enhanced microchannels of microchannel heat sinks." *International Journal of Heat and Mass Transfer* 175 (2021): 121332. <https://doi.org/10.1016/j.ijheatmasstransfer.2021.121332>
- [17] He, Kun, Ben Ma, and Lei Wang. "Electrohydrodynamic enhancement of phase change material melting in cylindrical annuli under microgravity." *Applied Thermal Engineering* 215 (2022): 119005. <https://doi.org/10.1016/j.applthermaleng.2022.119005>

- [18] Ajeeb, Wagd, Monica S. A. Oliveira, Nelson Martins, and S. M. Sohel Murshed. "Forced convection heat transfer of non-Newtonian MWCNTs nanofluids in microchannels under laminar flow." *International Communications in Heat and Mass Transfer* 127 (2021): 105495. <https://doi.org/10.1016/j.icheatmasstransfer.2021.105495>
- [19] Huang, Mengmeng, Chunying Zhu, Taotao Fu, and Youguang Ma. "Enhancement of gas-liquid mass transfer by nanofluids in a microchannel under Taylor flow regime." *International Journal of Heat and Mass Transfer* 176 (2021): 121435. <https://doi.org/10.1016/j.ijheatmasstransfer.2021.121435>
- [20] Wang, Hongyan, Mingxin Pang, Yanhua Diao, and Yaohua Zhao. "Heat transfer characteristics and flow features of nanofluids in parallel flat minichannels." *Powder Technology* 402 (2022): 117321. <https://doi.org/10.1016/j.powtec.2022.117321>
- [21] Peng, X. F., and G. P. Peterson. "Convective heat transfer and flow friction for water flow in microchannel structures." *International Journal of Heat and Mass Transfer* 39, no. 12 (1996): 2599-2608. [https://doi.org/10.1016/0017-9310\(95\)00327-4](https://doi.org/10.1016/0017-9310(95)00327-4)
- [22] Kline, Stephen J., and F. A. McClintock. "Describing uncertainties in single-sample experiments." *Mechanical Engineering* 75 (1963): 3-8.
- [23] Xian, Hong Wei, Rahman Saidur, Nor Azwadi Che Sidik, and Yutaka Asako. "Viscosity of CuO Nanofluid Due to Nanoparticles Size and Concentration." *Journal of Advanced Research in Applied Sciences and Engineering Technology* 28, no. 1 (2022): 161-167. <https://doi.org/10.37934/araset.28.1.161167>
- [24] Loon, Yew Wai, and Nor Azwadi Che Sidik. "A comprehensive review of recent progress of nanofluid in engineering application: Microchannel heat sink (MCHS)." *Journal of Advanced Research in Applied Sciences and Engineering Technology* 28, no. 2 (2022): 1-25. <https://doi.org/10.37934/araset.28.2.125>
- [25] Aman, Sidra, Dennis Ling Chuan Ching, Mohd Zuki Salleh, and Zulhibri Ismail. "Heat Generation Effects on Maxwell Nanofluid Passing Over an Oscillating Vertical Plate." *Journal of Advanced Research in Applied Sciences and Engineering Technology* 28, no. 2 (2022): 348-355. <https://doi.org/10.37934/araset.28.2.348355>
- [26] Ishak, Siti Shuhada, Nurul Nurfatihah Mazlan, Mohd Rijal Ilias, Roselah Osman, Abdul Rahman Mohd Kasim, and Nurul Farahain Mohammad. "Radiation Effects on Inclined Magnetohydrodynamics Mixed Convection Boundary Layer Flow of Hybrid Nanofluids over a Moving and Static Wedge." *Journal of Advanced Research in Applied Sciences and Engineering Technology* 28, no. 3 (2022): 68-84. <https://doi.org/10.37934/araset.28.3.6884>
- [27] Hanafi, Abdul Ghafur, Mohd Nasrun Mohd Nawawi, Mohd Kamarul Irwan Abdul Rahim, Faizatul Akmar Abdul Nifa, Mohd Faizal Omar, and Othman Mohamed. "Project managers selection in the construction industry: Towards the integration with artificial emotional intelligence and technology." *Journal of Advanced Research in Applied Sciences and Engineering Technology* 29, no. 1 (2022): 160-176. <https://doi.org/10.37934/araset.29.1.160176>
- [28] Mahat, Rahimah, Sharidan Shafie, and Imran Ullah. "Free convection of viscoelastic nanofluid flow on a horizontal circular cylinder with constant heat flux." *Journal of Advanced Research in Applied Sciences and Engineering Technology* 30, no. 3 (2023): 1-8. <https://doi.org/10.37934/araset.30.3.18>
- [29] Jowsey, Mohamad Hafzan Mohamad, Natrah Kamaruzaman, and Mohsin Mohd Sies. "Heat and Flow Profile of Nanofluid Flow Inside Multilayer Microchannel Heat Sink." *Journal of Advanced Research in Micro and Nano Engineering* 4, no. 1 (2021): 1-9.